CLOSING REPORT

Quant-ERA: Spin-based nanolytics – Turning today's quantum technology research frontier into tomorrow's diagnostic devices

Project period: 03/01/2018 – 10/31/2021

Total NKFIH budget: 48,000,000 HUF

PI, Consortium Partner: Dr. Ádám Gali (Wigner Research Centre for Physics)

Consortium Leader: Prof. Jens Anders (Stuttgart University)

Consortium Partners: Dr. Ilai Schwartz (NVision GmbH)

Prof. Fedor Jelezko (Ulm University)

Prof. Milos Nesladek (Hasselt University)

Dr. Petr Cigler (The Czech Academy of Sciences)

Dr. Adrik Welders (Wageningen University)

Prof. Martin Plenio (Ulm University)

Abstract: The goal of NanoSpin is to utilize an entirely novel approach towards spin-based analytics which uses diamond and silicon carbide based quantum technologies as its key element. Realizing this goal requires the combination of leading expertise from widely different disciplines including theoretical and experimental quantum physics, chemistry, material science and engineering. Thanks to the interdisciplinary nature of our team, we are able to provide the required theoretical, experimental, sensor- and instrumentation-related building blocks to achieve an overall performance greatly beyond the current state-of-the-art. More specifically, NanoSpin will leverage the immense power associated with color centers in (nano)diamonds and silicon carbide to establish the new discipline of nanoscale-NMR and enable dynamic hyperpolarization with unprecedented enhancement factors.

Wigner Research Centre for Physics will carry out *ab initio* simulations on color centers in silicon carbide and realize silicon carbide nanoparticles towards quantum sensing.

Date: 12/30/2021

Signature: Dr. Ádám Gali, PI

Introduction

In this project, Ádám Gali's group focused the investigation on silicon carbide (SiC) related defect quantum bits because silicon carbide is considered to be a bioinert material (e.g., Refs. [1,2]) and it is then expected that SiC quantum sensors can be directly applied *in vivo* and in human studies for diagnostic or therapeutic applications.

Ádám Gali's group's activities can be divided to two major thrusts:

i) Theoretical analysis of known or novel defect quantum bits by group theory, rate equations for the quantum optics control, and *ab initio* modeling for magneto-optical parameters required for the tight control and quantum sensor and related applications;

ii) Realize quantum defects in SiC nanoparticles and study its interaction in realistic biological environment for future quantum biosensor applications.

The investigations were realized in cooperation with the consortium partners and other partners where the most important partners outside the consortium in the USA (Prof. David D. Awschalom group), China (Dr. Jin-Shi Xu), and Czechia (Dr. Marie Kalbacova) are highlighted.

Methods

Theory

We applied *ab initio* methods to calculate the electronic structure of color centers which is based on supercell plane wave density functional theory methods (see Ref. [3] and references therein). The color centers were modeled by 576-atom or larger supercell. Viktor Ivády, Igor Abrikosov and Ádám Gali wrote a comprehensive review paper about the *ab initio* calculation of spin properties of solid-state defect quantum bits [3], which is a reference to methodologies applied in the project.

The calculations were carried out on massively parallelized computer clusters with the use of both local facilities, national (KIFÜ) and international supercomputer centers.

Experiment

Silicon carbide (SiC) large particles were prepared by self-propagated high-temperature synthesis in an induction furnace then stain etching is applied to create porous layers. Ultrasonication is applied then to cut the particles from the porous SiC material and finally colloid ultrasmall SiC nanoparticles (NPs) are formed. Detailed description can be found in Refs. [1,4].

We purchased devices to create and analysis the solubility and magneto-optical properties of SiC NPs. In particular, we bought a Zetasizer equipment to measure the zeta-potential of the SiC NPs as a major investment in the project which is critical in biological applications. Beside we purchased small equipment and a laptop to post-process the data from the analysis.

Results

Theory

Divacancy quantum bits in silicon carbide

We investigated the quenching of the photoluminescence (PL) from the divacancy defect in 4H silicon carbide (SiC) consisting of a nearest-neighbor silicon and carbon vacancies. The quenching occurs only when the PL is excited below certain photon energies (thresholds), which differ for the four different inequivalent divacancy configurations in 4H-SiC. An accurate theoretical *ab initio* calculation for the charge-transfer levels of the divacancy shows very good agreement between the position of the (0/−) level with respect to the conduction band for each divacancy configuration and the corresponding experimentally observed threshold, allowing us to associate the PL decay with conversion of the divacancy from neutral to negative charge state due to capture of electrons photoionized from other defects (traps) by the excitation [5]. We note that we applied *ab initio* many-body perturbation theory to the electron-phonon coupling on hexagonal silicon carbide (SiC) crystals and determine the temperature dependence of the bands. We found a significant electron-phonon renormalization of the band gap at 0 K but the temperature dependence of the conduction band minimum is tiny between 0 K and room temperature and does not contribute to the photoionization threshold [6]. Furthermore, we identified the different configurations of the divacancy defects to each of the QL1-QL6 color centers in 6H-SiC, respectively. We accomplished this by comparing the results from *ab initio* calculations with experimental measurements for the zero-phonon line, hyperfine tensor, and zero-field splitting [7].

Cubic silicon carbide (3C-SiC) is an excellent platform for integration of defect qubits into established wafer-scale device architectures for quantum information and sensing applications, where a divacancy qubit, which is similar to the negatively charged nitrogen-vacancy (NV) center in diamond, has favorable coherence properties. We demonstrated by means of density-functional-theory calculations that for most types of distortion the 3C-SiC divacancy exhibits slightly smaller spin-strain coupling parameters but greater spin-stress coupling parameters in comparison with the diamond NV. We predicted that high-quality 3C-SiC thin films hosting divacancy qubits are prospective platforms for quantum-enhanced pressure-sensor devices [8].

Interfacing solid-state defect electron spins to other quantum systems is an ongoing challenge. The ground-state spin's weak coupling to its environment not only bestows excellent coherence properties but also limits desired drive fields. The excited-state orbitals of these electrons, however, can exhibit stronger coupling to phononic and electric fields. We demonstrated electrically driven coherent quantum interference in the optical transition of single, basally oriented divacancies in commercially available 4H-SiC. By applying microwave frequency electric fields, we coherently drove the divacancy's excited-state orbitals and induce Landau-Zener-Stückelberg interference fringes in the resonant optical absorption spectrum. In addition, we found remarkably coherent optical and spin subsystems enabled by the basal divacancy's symmetry as derived from *ab initio* modeling [9]. These properties establish divacancies as strong candidates for quantum communication and hybrid system applications, where simultaneous control over optical and spin degrees of freedom is paramount.

Defect-based quantum systems in wide bandgap semiconductors are strong candidates for scalable quantum-information technologies. However, these systems are often complicated by charge-state instabilities and interference by phonons, which can diminish spin-initialization fidelities and limit room-

temperature operation. We identified a pathway around these drawbacks by showing that an engineered quantum well can stabilize the charge state of a qubit. Using density-functional theory and experimental synchrotron X-ray diffraction studies, we constructed a model for previously unattributed point defect centers in silicon carbide as a near-stacking fault axial divacancy and show how this model explains these defects' robustness against photoionization and room temperature stability. These results provide a materials-based solution to the optical instability of color centers in semiconductors, paving the way for the development of robust single-photon sources and spin quantum bits [10].

Spin defects in silicon carbide (SiC) with mature wafer-scale fabrication and micro/nano-processing technologies have recently drawn considerable attention. Although room temperature single-spin manipulation of color centers in SiC has been demonstrated, the typically detected contrast is less than 2%, and the photon count rate is also low. Here, we present the coherent manipulation of single divacancy spins in 4H–SiC with a high readout contrast (−30%) and a high photon count rate (150 kilo counts per second) under ambient conditions, which are competitive with the NV centers in diamond. Coupling between a single defect spin and a nearby nuclear spin is also observed. We further provided a theoretical explanation for the high readout contrast by analyzing the defect levels and decay paths [11]. Since the high readout contrast is of utmost importance in many applications of quantum technologies, this work might open a new territory for SiC-based quantum devices with many advanced properties of the host material.

Silicon-vacancy center in hexagonal silicon carbide

Scalable spin-to-photon interfaces require quantum emitters with strong optical transition dipole moment and low coupling to phonons and stray electric fields. It is known that particularly for coupling to stray electric fields, these conditions can be simultaneously satisfied for emitters that show inversion symmetry. We showed that inversion symmetry is not a prerequisite criterion for a spectrally stable quantum emitter. We found that identical electron density in ground and excited states can eliminate the coupling to the stray electric fields. Further, a strong optical transition dipole moment is achieved in systems with altering sign of the ground and excited wavefunctions. We used density functional perturbation theory to investigate an optical center that lacks of inversion symmetry, namely, the Si-vacancy color center in 4H-SiC. Our results showed that this system close to ideally satisfies the criteria for an ideal quantum emitter. Our study opens a novel rationale in seeking promising materials and point defects towards the realisation of robust spin-to-photon interfaces [12].

Scalable quantum networking requires quantum systems with quantum processing capabilities. Solid state spin systems with reliable spin–optical interfaces are a leading hardware in this regard. However, available systems suffer from large electron–phonon interaction or fast spin dephasing. We demonstrated that the negatively charged silicon-vacancy center in SiC is immune to both drawbacks. Thanks to its $^4A_2$ symmetry in ground and excited states, optical resonances are stable with near-Fourier-transform-limited linewidths, allowing exploitation of the spin selectivity of the optical transitions. In combination with millisecond-long spin coherence times originating from the high-purity crystal, we demonstrated high-fidelity optical initialization and coherent spin control, which we exploited to show coherent coupling to single nuclear spins with ∼1 kHz resolution. The summary of our findings makes this defect a prime candidate for realizing memory-assisted quantum network applications using semiconductor-based spin-to-photon interfaces and coherently coupled nuclear spins [13].

We explored the effect of temperature and strain on the fluorescence by focusing on the two silicon-vacancy qubits, V1 and V2, in 4H-SiC. We applied density-functional theory beyond the Born-Oppenheimer approximation to describe the temperature-dependent mixing of electronic excited states assisted by phonons. We obtained a polaronic gap of around 5 and 22 meV for the V1 and V2 centers, respectively, which results in a significant difference in the temperature-dependent dephasing and zero-field splitting of the excited states, which explains recent experimental findings. We also computed how crystal deformations affect the zero-phonon line of these emitters [14]. Our predictions are important ingredients in any quantum applications of these qubits sensitive to these effects. Indeed, we investigated the silicon vacancy centre in silicon carbide and demonstrated controlled emission of indistinguishable and distinguishable photons via coherent spin manipulation. Using strong off-resonant excitation and collecting zero-phonon line photons, we showed a two-photon interference contrast close to 90% in Hong-Ou-Mandel type experiments. Further, we exploited the system's intimate spin-photon relation to spin-control the color and indistinguishability of consecutively emitted photons. Our results provided a deep insight into the system's spin-phonon-photon physics and underlined the potential of the industrially compatible SiC platform for measurement-based entanglement distribution and photonic cluster state generation [15].

Optically addressable solid-state color center spin qubits have become important platforms for quantum information processing, quantum networks and quantum sensing. The readout of color center spin states with optically detected magnetic resonance (ODMR) technology is traditionally based on Stokes excitation, where the energy of the exciting laser is higher than that of the emission photons. We investigated an unconventional approach using anti-Stokes excitation to detect the ODMR signal of Si-vacancy defect spin in SiC, where the exciting laser has lower energy than the emitted photons. Laser power, microwave power and temperature dependence of the anti-Stokes excited ODMR are systematically studied, in which the behavior of ODMR contrast and linewidth is shown to be similar to that of Stokes excitation. However, the ODMR contrast is several times that of the Stokes excitation. Coherent control of Si-vacancy spin under anti-Stokes excitation is then realized at room temperature. The spin coherence properties are the same as those of Stokes excitation, but with a signal contrast that is around three times greater. To illustrate the enhanced spin readout contrast under anti-Stokes excitation, we also provided a theoretical model. The experiments demonstrated that the current anti-Stokes excitation ODMR approach has promising applications in quantum information processing and quantum sensing [16].

Crystallographic defects such as vacancies and stacking faults engineer electronic band structure at the atomic level and create zero- and two-dimensional quantum structures in crystals. The combination of these point and planar defects can generate a new type of defect complex system as we proved for divacancy defects previously [10]. We investigated SiC nanowires that host point defects near stacking faults. These point–planar defect complexes in the nanowire exhibit outstanding optical properties of high-brightness single photons (>360 kcounts/s), a fast recombination time (<1 ns), and a high Debye–Waller factor (>50%). These distinct optical properties of coupled point-planar defects lead to an unusually strong zero-phonon transition, essential for achieving highly efficient quantum interactions between multiple qubits. Our findings can be extended to other defects in various materials and therefore offer a new perspective for engineering defect qubits.

Furthermore, we identified the different configurations of the Si-vacancy defects to each of the V1, V2, and V3 color centers in 6H-SiC, respectively. We accomplished this by comparing the results from *ab initio*

calculations with experimental measurements for the zero-phonon line, hyperfine tensor, and zero-field splitting [7].

Other color centers in silicon carbide

The SiC/SiO$_2$ interface is a central component of many SiC electronic devices. Defects intrinsic to this interface can have a profound effect on their operation and reliability. It is therefore crucial to both understand the nature of these defects and develop characterization methods to enable optimized SiC-based devices. Here we make use of confocal microscopy to address single SiC/SiO$_2$-related defects and show the technique to be a noncontact, nondestructive, spatially resolved and rapid means of assessing thequality of the SiC/SiO$_2$ interface. This is achieved by a systematic investigation of the defect density of the SiC/SiO$_2$ interface by varying the parameters of a nitric oxide passivation anneal after oxidation. Standard capacitance-based characterization techniques are used to benchmark optical emission rates and densities of the optically active SiC/SiO$_2$-related defects. Further insight into the nature of these defects is provided by low-temperature optical measurements on single defects. Ádám Gali contributed to associate the high local vibration modes with carbon clusters at the SiC/SiO$_2$ interface [17].

Recently, vacancy-related spin defects in silicon carbide (SiC) have been demonstrated to be potentially suitable for versatile quantum interface building and scalable quantum network construction. Significant efforts have been undertaken to identify spin systems in SiC and to extend their quantum capabilities using large-scale growth and advanced nanofabrication methods. We demonstrated a type of spin defect in the 4H polytype of SiC generated via hydrogen ion implantation with high-temperature post-annealing, which is different from any known defects. These spin defects can be optically addressed and coherently controlled even at room temperature, and their fluorescence spectrum and optically detected magnetic resonance spectra are different from those of any previously discovered defects. Moreover, the generation of these defects can be well controlled by optimizing the annealing temperature after implantation. These defects demonstrate high thermal stability with coherently controlled electron spins, facilitating their application in quantum sensing and masers under harsh conditions [18].

Furthermore, we studied the optical properties of tetravalent-vanadium impurities in 4H SiC. Light emission from two crystalline sites is observed at wavelengths of 1.28 and 1.33 µm, with optical lifetimes of 163 and 43 ns, respectively, which remains stable up to 50 and 20 K, respectively. Moreover, spectrally broad photoluminescence is observed up to room temperature. Group-theory and *ab initio* density-functional supercell calculations enabled unequivocal site assignment and shed light on the spectral features of the defects. Specifically, our numerical simulations indicate that the site assignment is reversed with respect to previous assumptions. Our calculations showed that vanadium in SiC has highly favorable properties for the generation of single photons in the telecommunication wavelength regime. Combined with the available electronic and nuclear degrees of freedom, vanadium presents all the ingredients required for a highly efficient spin-photon interface [19].

Vanadium defect spin in 4H SiC exhibits interesting physics. In particular, character of wave functions and electron-phonon coupling in this defect may highly influence their interaction with external magnetic fields. Complex interplay among the electronic orbitals, phonons, and electron spin determines the effective pseudospin of the system that we demonstrated on vanadium and molybdenum defects in hexagonal SiC by means of *ab initio* calculations. We found a giant anisotropy in the g-tensor of these defects with Kramers doublet spin ground state, resulting in reduced and vanishing interaction with the magnetic field in parallel and transverse directions, respectively [20].

Experiments: silicon carbide nanoparticles

We studied the functionalization of SiC NPs towards biological applications and tested its toxicity. Furthermore, we introduced color centers into SiC NPs to form ultimate bioinert and molecular-sized quantum sensors.

Ultrasmall silicon carbide nanoparticles (SiC USNPs) are very promising biomarkers for developing new applications in diagnostics, cell monitoring or drug delivery, even though their interaction with biological molecules such as different proteins has not yet been investigated in detail. The biological behavior of SiC USNPs in a medium modeling a living organism was investigated in detail through the dependence of the fluorescence on interactions between bovine serum albumin (BSA) and SiC USNPs. The interaction showed transient nanoparticle–protein associations due to the restricted diffusion behavior of the nanoparticles in the vicinity of a protein. The transient association manifests in a complex fluorescence quenching mechanism where the dynamic component was dominated by Förster resonance energy transfer. By studying SiC nanoparticles of different sizes, it can be concluded that the transient effect is an ultrasmall nanoparticle behavior [1].

Ultra-small nanoparticles with sizes comparable to those of pores in the cellular membrane possess significant potential for application in the field of biomedicine. Silicon carbide ultra-small nanoparticles with varying surface termination were tested for the biological system represented by different human cells (using a human osteoblastic cell line as the reference system and a monocyte/macrophage cell line as immune cells). The three tested nanoparticle surface terminations resulted in the observation of different effects on cell metabolic activity. These effects were mostly noticeable in cases of monocytic cells, where each type of particle caused a completely different response ('as-prepared' particles, i.e., were highly cytotoxic, –OH terminated particles slightly increased the metabolic activity, while –NH$_2$ terminated particles caused an almost doubled metabolic activity) after 24 h of incubation. Subsequently, the release of cytokines from such treated monocytes and their differentiation into activated cells was determined. The results revealed the potential modulation of immune cell behavior following stimulation with particular ultra-small nanoparticles, thus opening up new fields for novel silicon carbide nanoparticle biomedical applications [2].

There is an urgent quest for room-temperature qubits in nanometer-sized, ultrasmall nanocrystals for quantum biosensing, hyperpolarization of biomolecules, and quantum information processing. Thus far, the preparation of such qubits at the nanoscale has remained futile. We presented a synthesis method that avoids any interaction of the solid with high-energy particles and uses self-propagated high-temperature synthesis with a subsequent electrochemical method, the no-photon exciton generation chemistry to produce room-temperature qubits in ultrasmall nanocrystals of sizes down to 3 nm with high yield. We first created the host SiC crystallites by high-temperature synthesis and then apply wet chemical etching, which results in ultrasmall SiC nanocrystals and facilitates the creation of thermally stable defect qubits in the material. We demonstrate room-temperature optically detected magnetic resonance signal of divacancy qubits with 3.5% contrast from these nanoparticles with emission wavelengths falling in the second biological window (1000–1380 nm). These results constitute the formation of nonperturbative bioagents for quantum sensing and efficient hyperpolarization [4]. We note that we also created divacancy quantum bits with the invasive neutron irradiation technique. We compared the optical properties of these divacancy defects with that of the non-invasive method aided by first principles simulations. Surprisingly, the recorded fluorescence spectra are similar in the two systems. The results were written up

in a paper and submitted to a special collection of the Journal of Applied Physics (under review) that we copied into the Appendix of the report.

The results above guided us how to stain etch 6H SiC which has not yet been achieved before. This can be important as many defect qubits were found in this polytype (e.g., Ref. [7]). We reported an electroless method to fabricate porous hexagonal silicon carbide and hexagonal silicon carbide nanoparticles (NPs) as small as 1 nm using wet chemical stain etching. We observed quantum confinement effect for ultrasmall hexagonal SiC NPs in contrast to the cubic SiC NPs. We attributed this difference to the various surface terminations of the two polytypes of SiC NPs [21].

Further, we showed that the SiC NPs can be integrated into classical semiconductor device. Colloidal cubic SiC nanocrystals were fabricated, characterized, and introduced into metal–insulator–semiconductor and metal–insulator–metal structures based on hafnium oxide layers. The fabricated structures were characterized through the stress-and-sense measurements in terms of device capacitance, flat-band voltage shift, switching characteristics, and retention time. The examined electrical performance of the sample structures has demonstrated the feasibility of the application of both types of structures based on SiC nanoparticles in memory devices [22].

Finally, X-ray-activated near-infrared luminescent nanoparticles are considered as new alternative optical probes due to being free of autofluorescence, while both their excitation and emission possess a high penetration efficacy *in vivo*. We reported SiC quantum dot sensitization of trivalent chromium-doped zinc gallate nanoparticles with enhanced near-infrared emission upon X-ray and UV–vis light excitation. We found that a $ZnGa_2O_4$ shell is formed around the SiC NPs during seeded hydrothermal growth, and SiC increases the emission efficiency up to 1 order of magnitude due to band alignment that channels the excited electrons to the chromium ion [23]. This X-ray activation can be very interesting for indirect excitation of SiC color centers that we wish to study in the near future.

Outlook

Despite on the pandemic crisis in the year of 2020, which forced us to elongate the project with eight months, significant results could be achieved. The results were published in prestigious journals, e.g. Nature Communications, Nature Partner Journal Quantum Information, Science Advances and National Science Review and also summarized in two review papers (one paper in Nature Partner Journal Computational Materials and one paper in Nature Materials Reviews). The published papers already received considerable number of citations (>100) and attracted great attention in the community of quantum technology researchers. The results were also presented in contributed and invited talks at workshops and conferences. Here we list the invited talks below. We note that because of the pandemic crisis the conference invitations were naturally ceased from 2020:

• *First principles calculation of highly anisotropic g-tensor of Kramers doublet transition metals in hexagonal SiC*, International Conference on Silicon Carbide and Related Materials 2019, Kyoto (Japan), September 28 - October 4, 2019

• *Ab initio study of defect qubits for hyperpolarization and quantum sensing*, Gordon Research Conference on Quantum Sensing, Hong Kong (China), June 2-6, 2019

- *Ab initio study of SiC qubits for hyperpolarization, quantum sensing and communication*, The Royal Society Theo Murphy Meeting on "SiC quantum spintronics: towards quantum devices in a technological material", Kavli Royal Society Centre, Chicheley Hall (UK), November 5-6, 2018

Young researchers were trained and worked in the project both in experiment and theory. The theorist, András Csóré, started to work as a PhD candidate on the project, and he could successfully defend his PhD thesis in 2020 (partially based on the project results) and continued to work on the project as postdoc researcher. The experimentalist, Gyula Károlyházy, continuously worked on the project as a PhD candidate where the majority of the thesis points is originated from the results achieved in the project. Gyula Károlyházy could successfully passed the pre-defense process and he has submitted the thesis for formal defense.

As a consequence of the results achieved by Ádám Gali's group and the overall consortium, new joint projects have been started with forming European research consortium for quantum technology calls. Furthermore, the methodology for creation of divacancy quantum bits in ultrasmall SiC NPs is completely novel and patent applications were submitted at national level (Nr. P1900269) in 2019 and at EPO (Nr. EP20187425) in 2020 that are still under review. We trust that our novel non-invasive method for creation vacancy-type defect quantum bits is a base of a new technology that can serve scientists and the quantum technology industry.

References (associated with the results of the project: see also references therein)

[1] G. Dravecz, T. Z. Jánosi, D. Beke, D. Á. Major, G. Károlyházy, J. Erostyák, K. Kamarás, and Á. Gali, *Identification of the Binding Site between Bovine Serum Albumin and Ultrasmall SiC Fluorescent Biomarkers*, Phys. Chem. Chem. Phys. **20**, 13419 (2018).

[2] T. Bělinová, I. Machová, D. Beke, A. Fučíková, A. Gali, Z. Humlová, J. Valenta, and M. Hubálek Kalbáčová, *Immunomodulatory Potential of Differently-Terminated Ultra-Small Silicon Carbide Nanoparticles*, Nanomaterials **10**, 3 (2020).

[3] V. Ivády, I. A. Abrikosov, and A. Gali, *First Principles Calculation of Spin-Related Quantities for Point Defect Qubit Research*, Npj Comput Mater **4**, 76 (2018).

[4] D. Beke, J. Valenta, G. Károlyházy, S. Lenk, Z. Czigány, B. G. Márkus, K. Kamarás, F. Simon, and A. Gali, *Room-Temperature Defect Qubits in Ultrasmall Nanocrystals*, J. Phys. Chem. Lett. **11**, 1675 (2020).

[5] B. Magnusson, N. T. Son, A. Csóré, A. Gällström, T. Ohshima, A. Gali, and I. G. Ivanov, *Excitation Properties of the Divacancy in $4H$-SiC*, Phys. Rev. B **98**, 195202 (2018).

[6] E. Cannuccia and A. Gali, *Thermal Evolution of Silicon Carbide Electronic Bands*, Phys. Rev. Materials **4**, 014601 (2020).

[7] J. Davidsson, V. Ivády, R. Armiento, T. Ohshima, N. T. Son, A. Gali, and I. A. Abrikosov, *Identification of Divacancy and Silicon Vacancy Qubits in 6H-SiC*, Appl. Phys. Lett. **114**, 112107 (2019).

[8] P. Udvarhelyi and A. Gali, *Ab Initio Spin-Strain Coupling Parameters of Divacancy Qubits in Silicon Carbide*, Phys. Rev. Applied **10**, 054010 (2018).

[9] K. C. Miao, A. Bourassa, C. P. Anderson, S. J. Whiteley, A. L. Crook, S. L. Bayliss, G. Wolfowicz, G. Thiering, P. Udvarhelyi, V. Ivády, H. Abe, T. Ohshima, Á. Gali, and D. D. Awschalom, *Electrically Driven Optical Interferometry with Spins in Silicon Carbide*, Science Advances **5**, eaay0527 (2019).

[10] V. Ivády, J. Davidsson, N. Delegan, A. L. Falk, P. V. Klimov, S. J. Whiteley, S. O. Hruszkewycz, M. V. Holt, F. J. Heremans, N. T. Son, D. D. Awschalom, I. A. Abrikosov, and A. Gali, *Stabilization of Point-Defect Spin Qubits by Quantum Wells*, Nat Commun **10**, 5607 (2019).

[11] Q. Li, J.-F. Wang, F.-F. Yan, J.-Y. Zhou, H.-F. Wang, H. Liu, L.-P. Guo, X. Zhou, A. Gali, Z.-H. Liu, Z.-Q. Wang, K. Sun, G.-P. Guo, J.-S. Tang, H. Li, L.-X. You, J.-S. Xu, C.-F. Li, and G.-C. Guo, *Room

Temperature Coherent Manipulation of Single-Spin Qubits in Silicon Carbide with a High Readout Contrast, National Science Review nwab122 (2021) DOI: 10.1093/nsr/nwab122.

[12] P. Udvarhelyi, R. Nagy, F. Kaiser, S.-Y. Lee, J. Wrachtrup, and A. Gali, *Spectrally Stable Defect Qubits with No Inversion Symmetry for Robust Spin-To-Photon Interface*, Phys. Rev. Applied **11**, 044022 (2019).

[13] R. Nagy, M. Niethammer, M. Widmann, Y.-C. Chen, P. Udvarhelyi, C. Bonato, J. U. Hassan, R. Karhu, I. G. Ivanov, N. T. Son, J. R. Maze, T. Ohshima, Ö. O. Soykal, Á. Gali, S.-Y. Lee, F. Kaiser, and J. Wrachtrup, *High-Fidelity Spin and Optical Control of Single Silicon-Vacancy Centres in Silicon Carbide*, Nature Communications **10**, 1954 (2019).

[14] P. Udvarhelyi, G. Thiering, N. Morioka, C. Babin, F. Kaiser, D. Lukin, T. Ohshima, J. Ul-Hassan, N. T. Son, J. Vučković, J. Wrachtrup, and A. Gali, *Vibronic States and Their Effect on the Temperature and Strain Dependence of Silicon-Vacancy Qubits in $4H$-$\mathrm{Si}\mathrm{C}$*, Phys. Rev. Applied **13**, 054017 (2020).

[15] N. Morioka, C. Babin, R. Nagy, I. Gediz, E. Hesselmeier, D. Liu, M. Joliffe, M. Niethammer, D. Dasari, V. Vorobyov, R. Kolesov, R. Stöhr, J. Ul-Hassan, N. T. Son, T. Ohshima, P. Udvarhelyi, G. Thiering, A. Gali, J. Wrachtrup, and F. Kaiser, *Spin-Controlled Generation of Indistinguishable and Distinguishable Photons from Silicon Vacancy Centres in Silicon Carbide*, Nature Communications **11**, 1 (2020).

[16] J.-F. Wang, F.-F. Yan, Q. Li, Z.-H. Liu, J.-M. Cui, Z.-D. Liu, A. Gali, J.-S. Xu, C.-F. Li, and G.-C. Guo, *Robust Coherent Control of Solid-State Spin Qubits Using Anti-Stokes Excitation*, Nat Commun **12**, 3223 (2021).

[17] B. C. Johnson, J. Woerle, D. Haasmann, C. T.-K. Lew, R. A. Parker, H. Knowles, B. Pingault, M. Atature, A. Gali, S. Dimitrijev, M. Camarda, and J. C. McCallum, *Optically Active Defects at the Si C / Si O 2 Interface*, Phys. Rev. Applied **12**, 044024 (2019).

[18] F.-F. Yan, A.-L. Yi, J.-F. Wang, Q. Li, P. Yu, J.-X. Zhang, A. Gali, Y. Wang, J.-S. Xu, X. Ou, C.-F. Li, and G.-C. Guo, *Room-Temperature Coherent Control of Implanted Defect Spins in Silicon Carbide*, Npj Quantum Inf **6**, 38 (2020).

[19] L. Spindlberger, A. Csóré, G. Thiering, S. Putz, R. Karhu, J. U. Hassan, N. T. Son, T. Fromherz, A. Gali, and M. Trupke, *Optical Properties of Vanadium in 4H Silicon Carbide for Quantum Technology*, Phys. Rev. Applied **12**, 014015 (2019).

[20] A. Csóré and A. Gali, *Ab Initio Determination of Pseudospin for Paramagnetic Defects in SiC*, Phys. Rev. B **102**, 241201 (2020).

[21] G. Károlyházy, D. Beke, D. Zalka, S. Lenk, O. Krafcsik, K. Kamarás, and Á. Gali, *Novel Method for Electroless Etching of 6H–SiC*, Nanomaterials **10**, 3 (2020).

[22] A. Mazurak, R. Mroczyński, D. Beke, and A. Gali, *Silicon-Carbide (SiC) Nanocrystal Technology and Characterization and Its Applications in Memory Structures*, Nanomaterials **10**, 12 (2020).

[23] D. Beke, M. V. Nardi, G. Bortel, M. Timpel, Z. Czigány, L. Pasquali, A. Chiappini, G. Bais, M. Rudolf, D. Zalka, F. Bigi, F. Rossi, L. Bencs, A. Pekker, B. G. Márkus, G. Salviati, S. E. Saddow, K. Kamarás, F. Simon, and A. Gali, *Enhancement of X-Ray-Excited Red Luminescence of Chromium-Doped Zinc Gallate via Ultrasmall Silicon Carbide Nanocrystals*, Chem. Mater. **33**, 2457 (2021).

Appendix (submitted paper)

Photoluminescence spectrum of divacancy in porous and nanocrystalline cubic silicon carbide

András Csóré,[1] Nain Mukesh,[2] Gyula Károlyházy,[2] David Beke,[1,2] and Adam Gali[1,2]

[1] *Department of Atomic Physics, Budapest University of Technology and Economics,*
Budafoki út 8., H-1111, Budapest, Hungary

[2] *Wigner Research Centre for Physics,*
PO. Box 49, Budapest H-1525, Hungary

(Dated: December 21, 2021)

Abstract

Divacancy in silicon carbide (SiC) is a prominent solid state defect quantum bit which bears a relatively strong fluorescence and optically detected magnetic resonance contrast (ODMR) at room temperature. These properties exemplify it for quantum sensing of biological molecules. To this end, we previously developed a top-down method to create divacancies in cubic SiC nanoparticles (NPs) as non-perturbative ODMR biomarkers. In this process, large SiC particles are synthesised and then stain etched to form porous SiC and then ultrasonication and filtering are applied to the solution to extract few nanometers diameter SiC NPs. We called this process as no-photon exciton generation chemistry (NPEGEC). We showed that adding aluminum to carbon and silicon in the synthesis process of cubic SiC, one can engineer divacancy defects in SiC NPs by NPEGEC. An alternative traditional way to introduce vacancies to the SiC lattice is irradiation. Here, we compare the fluorescence spectra of divacanies as created by neutron irradiation in porous cubic SiC and NPEGEC technique in SiC NPs, and the results are analyzed in detail by means of first principles calculations. We find that the irradiation technique produces a larger shift in the fluorescence spectrum with residual background fluorescence than that for divacancies in SiC NPs which is most likely caused by the parasitic defects left after irradiation and annealing in the former sample. These results imply that the chemistry technique applied to prepare divacancies in few nanometers SiC NPs may preserve the bulk-like quality of divacancy quantum bits near the surface.

I. INTRODUCTION

Solid state point defects exhibiting paramagnetic electronic ground and optical excited state are forefront contenders as building blocks of certain quantum technology devices [1, 2]. In particular, defects in silicon carbide (SiC) are applicable as single-photon emitters being pivotal in quantum information processing [3–7], ultrasensitive nanosensors in magnetometry [8–13] or thermometry[9, 14] and quantum bits (qubits) [15, 16]. The divacancy ($V_C V_{Si}$) in SiC — consisting of a silicon vacancy (V_{Si}) and a neighboring carbon vacancy (V_C) — is an outstanding member of the wide palette of SiC defects. $V_C V_{Si}$ in SiC exhibits several desirable properties making it a promising qubit candidate. In particular, its electronic structure introduces spin triplet ($S{=}1$) ground and optical excited states [15, 17–21].

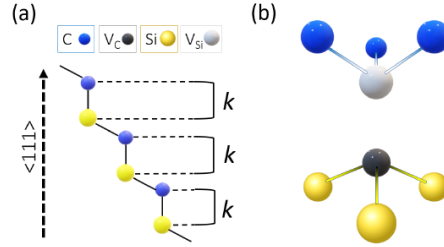The corresponding optical transitions, i.e. the zero-phonon lines (ZPL) are around

2

Figure 1. (a) Lattice structure of the perfect 3C SiC. Crystal direction of $\langle 111 \rangle$ is indicated. (b) Microscopic structure of the divacancy defect. Color code of atoms is indicated. We note that the symmetry axis of divacancy is pointing along the $\langle 111 \rangle$ axis of the crystal.

1100 nm with relatively long-tail phonon sideband up to 1400 nm falling into the near-infrared (NIR) region [16, 22–24]. In particular, the majority of emission band fall to the so-called second biological window [25] where the absorption and autofluorescence of water and biological molecules are minimal. This property makes the divacancy color center in small SiC nanocrystal desirable candidate as an ultrasensitive biomarker [26–28].

We focus our attention to the cubic SiC or 3C SiC matrix hosting the divacancy defect (see Fig. 1) because divacancy centers were prepared in such polytype of SiC in nanocrystalline form [28]. We note that the coherence times and fluorescence properties of divacancy quantum bits in 3C SiC are all favorable similar to its counterparts in other polytypes of SiC [16], however, its optical properties are largely unexplored, in particular, in porous and nanocrystalline 3C SiC matrix.

In this brief report, we study the room temperature divacancy fluorescence spectrum from neutron irradiated and annealed porous SiC as well as from such few nanometers diameter SiC NPs that were created by chemistry without any invasive techniques towards the crystal structure. We apply Kohn-Sham spinpolarized density functional theory (DFT) calculations in 3C SiC to analyse the data. The theory starts with the temperature-dependent spectrum with comparing the results with literature data in bulk 3C SiC at cryogenic temperatures. The fluorescence or photoluminescence (PL) lineshape is approximated by the Huang-Rhys (HR) theory [29–31]. Our paper is organized as follows: we describe the preparation of divacancy defects in porous and nanocrystalline 3C SiC, the calculation method of the photoluminescence lineshape and the DFT simulation parameters in in Sec. II. We report and discuss our results with starting the theoretical description and continuing with comparison

to experimental data in Sec. III. Our conclusions are summarized in Sec. IV.

II. METHODOLOGY

A. Experimental setup

The preparation and characterization of SiC nanoparticles (NPs) containing $V_C V_{Si}$ centers was already reported by us [28]. Briefly, Si (99%, 325 mesh, Sigma Aldrich) and C [Norit A supra, surface area (BET), 1700 m^2/g] in 1:1 ratio and 3 wt% PTFE (Polytetrafluoroethylene) (1 μm particle size, Sigma Aldrich), 5 wt% Al powder (95%, <5 μm, Sigma Aldrich) were mixed in a ball mill for 12 hours to prepare SiC powder. The mixture was placed into a graphite crucible and annealed to about 1250 °C in an argon atmosphere for 8 minutes using an induction furnace (Stanelco STX25-DF1, 9.5 kV, 3.5 A, 288 kHz). The samples were then annealed at 650 °C in air for 10 hours and etched with HNO_3:H_2O 1:1 and HF:HNO_3:H_2O 1:1:10 in order to remove unreacted carbon, Al, and Si. Cubic SiC NPs were prepared from SiC powders via the no-photon exciton generation (NPEGEC) method [32] as follows. 5 g of SiC was etched in 40 ml HF:HNO_3 3:1 mixture at 180 °C using a high-pressure acid digestion chamber (DAB-3, 250 ml, Berghoff GmbH) to create porous SiC NPs. The porous SiC was either neutron-irradiated (1018 n/cm^2 0.18-2.5 MeV, TRIGA Mark II Reactor, TU Vienna) and annealed at 750 °C for 2 hours to create divacancies in the nanostructure, or was sonicated in DI water for 3 hours, then centrifuged at 8500 rpm for 40 minutes to create SiC NPs in size range of 4-6 nm. The supernatant contains the nanoparticles. To remove most of the larger or smaller particles, the supernatant was filtered through a 0.1 μm syringe filter, a 20 nm syringe filter (Whatman® Anotop® 10, Sigma Aldrich), and a Pall Macrosep 100 kDa centrifuge filter. A Pall Macrosep, 10 kDa filter, was used to remove species smaller than 3 nm, and finally, the retentate was used. The retentate was diluted with DI water and sonicated for 30 minutes. In the case of the NPs, 140 °C annealing was applied for 2 hours.

Fluorescence spectra were recorded at room temperature with Horiba Jobin-Yvon NanoLog FL3-2iHR spectrophotometer equipped with an iHR-320 grating spectrometer and a Symphony liquid-nitrogen cooled InGaAs CCD. A Roithner RLTMDL-785-1W-1 laser was used for 785-nm excitation. The applied power was 250 mW, and the spot size was about 15 mm.

4

Samples were drop casted on a Si or a quartz substrate.

B. Huang-Rhys theory of the PL spectrum

The PL emission spectrum including phonon-assisted electronic transitions were obtained by applying the Huang-Rhys (HR) [29] theory as implemented by Gali *et al.* [31]. The strength of the electron-phonon coupling is represented by the HR factor $[S(\hbar\omega)]$. Detailed derivation of S can be found in Refs. [30, 31, 33]. The S factor has intimate connection to the Debye-Waller (DW) factor (w) [34, 35] which is the ratio of the ZPL intensity and the total intensity that can be directly read from the experimental spectrum (if there are no overlapping spectra in the critical wavelength region). The relation between the two is $w = \exp(-S)$.

We provide here the key equations to generate the fluorescence or photoluminescence (PL) lineshape. The PL spectrum $[I^{\text{EM}}(\hbar\omega)]$ can be expressed as [30]

$$I^{\text{EM}}(\hbar\omega) = C^{\text{EM}}\omega^3\mu_{\text{EG}}^2 \sum_{n,m} \left|\left\langle\Theta_{\text{ES}}^m(Q)\middle|\Theta_{\text{GS}}^n(Q)\right\rangle\right|^2 \delta(E_{\text{ES}}^m - E_{\text{GS}}^n - \hbar\omega), \qquad (1)$$

where the transitions from the corresponding vibronic substates of the excited state (ES), indexed by m, to those of the ground state (GS) with the index n are also considered establishing the phonon sideband (PSB) besides the ZPL. If $m = n = 0$, $I^{\text{EM}}(\hbar\omega)$ yields the intensity of ZPL. In Eq. 1 $\boldsymbol{\mu}_{\text{EG}}$ is the corresponding matrix element (which is now a three component vector with the length of μ_{EG}) of the transition dipole moment operator, $\hat{\boldsymbol{\mu}}_{\text{EG}} = q\sum_j \hat{\mathbf{r}}_j$ defined as

$$\boldsymbol{\mu}_{\text{EG}} = \left\langle\Psi_{\text{ES}}(\mathbf{r}_i)\middle|\hat{\boldsymbol{\mu}}_{\text{EG}}\middle|\Psi_{\text{GS}}(\mathbf{r}_i)\right\rangle. \qquad (2)$$

and $\hbar\omega$ is the photon energy. The prefactor ω^3 in Eq. 1 consists of the photon density of states (DOS) causing spontaneous emission $(\sim \omega^2)$ and the perturbing field of those photons $(\sim \omega)$. In contrast, the absorption spectrum is a linear function of ω since no spontaneous emission is involved. In Eq. 1 C^{EM} is a constant which depends on materials and technicalities of the measurements. Since C^{EM} and $\hat{\boldsymbol{\mu}}_{\text{EG}}$ are constants across the spectrum, we used Eq. 3 as the PL lineshape $[L^{\text{EM}}(\hbar\omega)]$ defined as

5

$$L^{\text{EM}}(\hbar\omega) = \omega^3 \sum_{n,m} \left| \left\langle \Theta^n_{\text{GS}}(Q) \middle| \Theta^m_{\text{ES}}(Q) \right\rangle \right|^2 \delta(E^m_{\text{ES}} - E^n_{\text{GS}} - \hbar\omega), \tag{3}$$

In Eqs. 1 and 3, the overlapping integral of the GS and ES vibrational states denoted by $\Theta^m_{\text{ES}}(Q)$ and $\Theta^n_{\text{GS}}(Q)$, respectively. The partial HR factor of ω_k vibration is associated with the overlap integral where the sum of partial HR factors yield the total HR factor S. At $T = 0$ K, the lowest energy phonon state is occupied in the electronic excited state, i.e., $m = 0$. As the temperature raised higher energy m phonon states are occupied. Boltzmann distribution function may be applied at elevated temperatures as the high temperature limit of the Bose-Einstein distribution function for calculating the occupation of ω_k phonon state. By this way, the temperature dependent PL lineshape may be obtained. We note that all HR spectra presented in this work are normalized.

The temperature dependent width of ZPL emission is not incorporated in this theory. Principally, the ZPL width is associated with the optical lifetime at $T = 0$ K for a single divacancy defect but may rapidly broaden at elevated temperatures for dynamic Jahn-Teller systems in the excited state. Indeed, the ^3E ES of divacancy is a dynamic Jahn-Teller state similarly to NV center in diamond which leads to a T^5 dependence for broadening the ZPL peak because of the Raman transition of acoustic phonons [36]. As no experimental data is available for the temperature dependent linewidth of the ZPL emission for divacancy in 3C SiC, we employ the theory from NV center in diamond but the prefactor before the T^5 dependence is estimated to be two orders of magnitude larger because SiC has much lower Debye-temperature than that of diamond. As a consequence, the broadening of ZPL line becomes 10 meV at room temperature. This could be a rough but plausibe approximation as the two systems are very similar to each other but with stronger temperature dependence in SiC than that in diamond [16, 20, 21].

C.   Computational methodology

In order to obtain the temperature dependent PL spectrum we calculated the ground and optical excited states by means of HSE06 range-separated hybrid functional [37] accompanied by ΔSCF method [38] in excited state calculations. The divacancy defect was modeled in a 512-atom 3C SiC supercell. Fully relaxed geometries were obtained by minimizing the

interatomic forces between using the threshold of 0.01 eV/Å. Kohn-Sham wavefunctions were expanded in plane wave basis set with the cutoff energy of 420 eV. In the calculations only valence electrons were treated explicitly, core-electrons were considered in the framework of projector augmented wave (PAW) method [39] as implemented in the Vienna Ab-Initio Simulation Package (VASP) [40].

In the excited state electronic structure, a strong electron-phonon coupling may emerge (see Sec. III A) which can be described as Jahn-Teller (JT) effect [41]. Accordingly, the symmetry will be reduced from C_{3v} to C_{1h} by coupling to phonons in order to split the corresponding e level lifting the degeneracy in total energy. In calculation of the emission spectrum we use static JT distorted geometries exhibiting the lowest total energy. For the vibrational modes, we calculated the dynamical matrix in the ground state containing the second order derivatives of the total energy by means of the Perdew-Burke-Ernzerhof (PBE) [42] functional.

For the analysis of the phonon sideband, we applied the inverse participation ratio (IPR) for quantifying the localization of quasilocal phonon modes [30, 43] defined as

$$\text{IPR}_k = \frac{N \sum_i \mathbf{u}_i^4}{\left(\sum \mathbf{u}_i^2\right)^2}, \tag{4}$$

where $\mathbf{u}_i$ is the vector displacement amplitude of the ith atom in the kth phonon mode and N is the number of atoms in the supercell that is N=512 in our case. Consequently, the IPR fall in the region of $[1, N]$. When all atoms participating in a phonon mode possess equal amplitudes in their motion, the IPR is equal to the number of atoms vibrating in the certain phonon mode.

III.   RESULTS AND DISCUSSION

The PL lineshape of divacancy in 3C SiC depends on the intricate details of the electronic structure of the defect in the ground state and the excited state electronic configurations as well as the change in the geometry upon illumination. Materials imperfections such as strain caused by either the presence of other nearby point defects or the surface for shallow lying divacancy defects may shift and broaden the PL spectrum which cause inhomogeneous broadening in the PL spectrum recorded for ensemble of divacancy defects. In high quality

chemical vapor deposited (CVD) 3C SiC layers the strain is less present, although, typically 3C SiC is grown on top of silicon substrate and the lattice mismatch between the substrate and 3C SiC layers may effect the PL spectrum of divacancy at deeper region in the host crystal far from the interface.

In first principles simulations, one can study the intrinsic nature of the emission of an isolated defect. Although, the concentration of divacancy defect in a 512-atom supercell is still much higher than that in experiments but the strain field generated by the defect decays at the Wigner-Seitz boundaries of the 512-atom supercell, thus it may be taken as nearly isolated in a perfect 3C SiC environment. Therefore, we apply the strategy that we first analyze the electronic structure and PL lineshape from first principles (Sec. III A) and compare the results to the highest quality PL spectrum of divacancy in CVD-grown 3C SiC layers at low temperature from Ref. 16 (Sec. III B) which is a reference PL spectrum of divacancy in 3C SiC. Here we extend the simulation towards elevated temperatures critical for biomarker applications. Finally, we report our experimental PL spectra on neutron irradiated porous 3C SiC and nanocrystalline 3C SiC NPs at room temperature with analysing the change in the spectrum with respect to the reference PL spectrum and its implication on the preparation of quantum sensors (Sec. III C).

A.   Electronic structure

The divacancy defect introduces an a_1 and a degenerate e level to the band gap (2.29 eV) as depicted in Fig. 2. In the ground state the lower-in-energy non-degenerate a_1 level is fully occupied by two electrons, while the double degenerate e level is occupied by two electrons with parallel spins establishing the $^3A_2$ spin triplet state. The optical excited state is formed by promoting an electron in the minority spin channel from the a_1 level to the degenerate e level yielding the $a_1(1)e(3)$ electronic configuration providing the many-body wavefunction of ^3E. However, fractional occupation of the e level may give rise to electron-phonon coupling described by the JT effect. In this way, the symmetry described by the C_{3v} point group will be reduced to C_{1h} symmetry lifting the degeneracy of the e level resulting in non-degenerate levels of a' and a''. The PL spectrum is calculated in the distorted geometry in the electronic excited state which then includes the contribution of e phonons in the phonon sideband [44].

8

B. Simulated temperature-dependent PL spectrum

In this Section we report the PL spectrum of the divacancy defect in 3C SiC. First, we discuss the $T =0$ K case depicted in Fig. 3 as obtained from DFT calculations. We note that we do not include here any inhomogeneous broadening, thus the simulated spectrum refers to the ideal case when all the defects are well isolated in a perfect 3C SiC environment. The calculated ZPL is located at 1.14 eV (1087.6 nm), while the corresponding experimental value is at 1.12 eV (1107.0 nm) [16] demonstrating the accuracy of the HSE06 functional in these calculations. We note that ZPL energy in 3C SiC is close to those of $V_C V_{Si}$ configurations in 4H SiC, varying from 1.10 eV to 1.15 eV [45, 46]. In Fig. 3, the simulated ZPL energy is aligned to the experimental value for the sake of direct comparison of the simulated and observed phonon sideband. The calculated HR factor $S = 2.71$ yields a DW factor of $w = 0.07$ which is a higher value than that for the divacancy defects in 4H SiC [33]. Indeed, low-temperature PL experiments confirm these results as $w = 0.073 \pm 0.003$ have been observed for divacancy in 3C SiC and a lower w values were detected for divacancy configurations in 4H SiC [16].

We note that the simulation does not include the long wavelength phonons because of the finite size of the supercell which requires an embedding method (e.g., Ref. 30), therefore, the S factor is a bit underestimated. The missing low wavelength phonons in the simulation lead to an atificial gap between the ZPL peak and the onset of phonon sideband (PSB). This could affect the simulated PL spectrum at elevated temperatures in terms of the appearance of ZPL peak. Another consequence of the finite supercell size in the PL spectrum is that relatively sharp peaks develop in the phonon sideband that might be smoothened. We applied 3 meV gaussian broadening around all peaks in the phonon sideband to mitigate this problem.
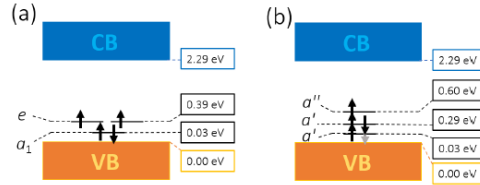

Figure 2. Single particle spectrum of (a) ground and (b) excited state. Electron spins are represented by black arrows, the reminiscent hole after the optical excitation is depicted as gray arrow.
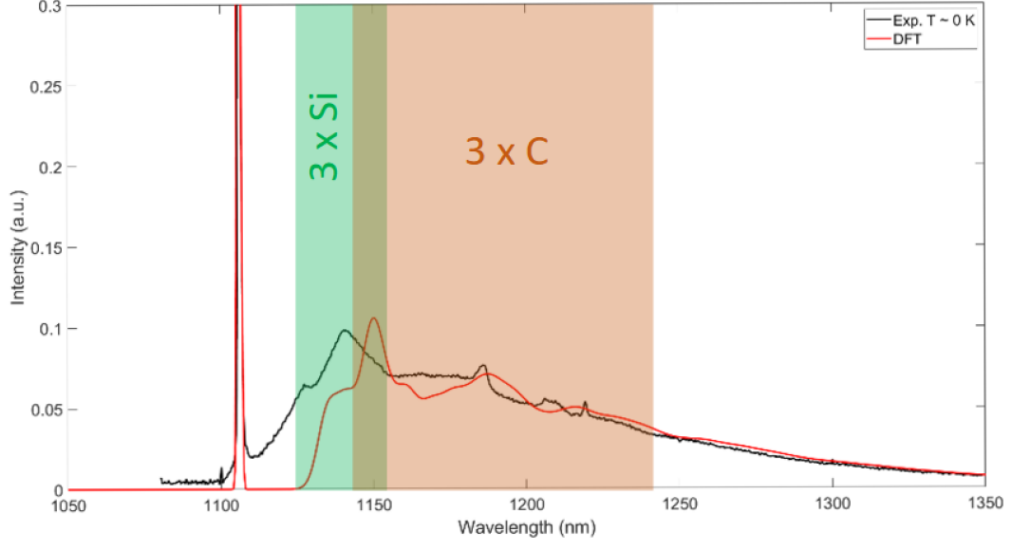
Figure 3. Calculated HR emission spectrum at $T = 0$ K. Energy of the phonon modes localized on the $3 \times$ Si atoms around the V_C falls in the $\approx 18 - 40$ meV region (green shaded area), while that of the $3 \times$ C atoms around V_{Si} falls into the $\approx 35 - 120$ meV region (orange shaded area).

Therefore, good agreement with experimental data could partially rely on cancellation of errors, nevertheless, our approach is well established for analysing the structure of PSB.

The PL spectrum of divacancy consists of a sharp ZPL with several longer wavelength (or smaller energy) peaks in the phonon sideband at T=0 K temperature. The ZPL and the onset of PSB is separated by a $\approx$15 meV gap and the broadening of the PSB is about 250 meV (about 300 nm). As we noted above the separation between the ZPL peak and the onset of PSB is an artifact of the supercell size which may also affect the position associated with the quasilocal phonon modes in the PL spectrum. We find a rich set of phonon-assisted optical transition mainly related to the phonons localized on the $3 \times$ C atoms around the V_{Si} and the $3 \times$ Si atoms around the V_C (cf. Fig. 1). Our IPR analysis implies that in the phonon energy region of $\approx 18 - 40$ meV (shift of 20-42 nm with respect to ZPL) the phonon modes mostly localized on the $3 \times$ Si atoms with the IPR of $\approx 1 - 5$, while phonon modes with energy falling in the $\approx 35 - 120$ meV (shift of 36-133 nm with respect to ZPL) region are mainly localized on the $3 \times$ C atoms atoms with similar IPR in the smulated spectrum which appears at about 10 nm shorter wavelength in the experimental spectrum. The strongest feature in the simulated PSB appears between $1160 - 1170$ meV (1060-1069 nm), i.e., in the
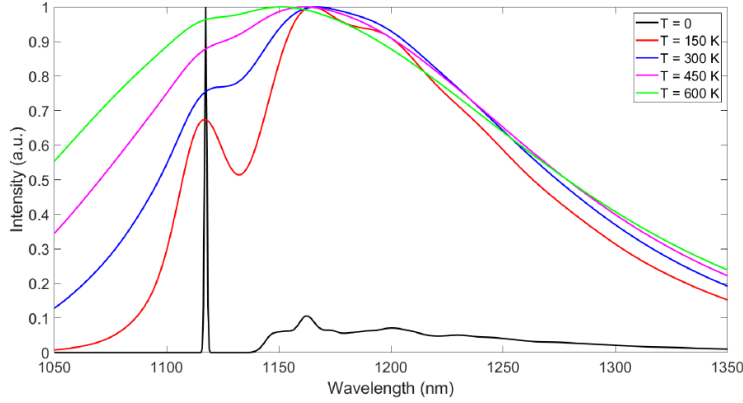
Figure 4. Calculated temperature-dependent HR emission spectrum at temperatures of 0 K (black line), 150 K (red line), 300 K (blue line), 450 K (magenta line) and 600 K (green line).

intersection of the $3 \times$ C and $3 \times$ Si phonon mode region (cf. Fig 3) demonstrating that phonon modes localized on both $3 \times$ C and $3 \times$ Si atoms contribute to this feature resulting at least twice as large amplitude as any other peaks in the PSB.

The numerical temperature-dependent emission spectrum is shown in Fig. 4. The emission spectrum was calculated at the temperatures of $T = \{0, 150, 300, 450, 600\}$ K. Amplitudes of sharp features in the PSB decrease by elevating the temperature and at 450 K they become almost entirely smeared in our simulation. The missing long wavelength phonons in the simulation will not broaden the spectrum around the ZPL peak which is an artifact of the supercell size. In experiments, the ZPL peak becomes almost invisible due to the broadening of the long wavelengths phonon bands. Nevertheless, the overall temperature broadening of the PL spectrum, in particular, the long wavelength tail, should be well described by our simulations.

We further note that the absorption spectrum is basically a mirror image of the PL spectrum which is mirrored vertically to the ZPL peak. This means that, by increasing the temperature, transition probability at lower than ZPL energies also increases providing the possibility of optical excitation at longer wavelength than ZPL energies, i.e., anti-Stokes excitation, that has been observed for Si-vacancy in 4H SiC [47].

11

C.   Room-temperature PL emission spectrum in porous and nanocrystalline cubic SiC

As divacancy consists of nearby Si-vacancy and C-vacancy, the obvious method to form this defect is to irradiate SiC crystal for kicking out the Si and C atoms from their crystalline positions and then apply annealing to create them (e.g., Ref. 24). In this process, the irradiation species should have enough energy to kick out the heavy silicon atoms beside the light carbon atoms. By appropriate annealing temperature, the vacancies starts to migrate and form complexes with each other where the simplest complex is the divacancy. However, not all the vacancies join in the process or they may form even larger complexes [24], thus parasitic defects of vacancy clusters, interstitial clusters and antisite complexes may coexist with divacancies with creating strain fields around the target divacancy defects. This will affect the PL spectrum and if they are paramagnetic then the spin properties of divacancies may be deteroirated. As a consequence, the PL spectrum for the ensemble of divacancies is an indicator about the possible overall performance of these divacancy qubits when referenced to the PL spectrum of divacancy in high quality cubic SiC or single defect measurements.

High quality formation of divacancies in SiC should attempt to avoid irradiation techniques. This scenario is not impossible by recognizing the fact that divacancies were observed in so-called high-purity semiinsulating (HPSI) 4H SiC (e.g., Ref. 15) which were grown by hot wall CVD process far from equilibrium process. On the other hand, high temperature growth of 3C SiC is not likely as high temperature prefers the formation of hexagonal SiC. However, our group has recently discovered that if Si-deficient 3C SiC is formed by adding aluminum or boron precursor in the growth process and surface carbon vacancy is introduced to the 3C SiC NPs by etching process then very low temperature annealing is able to transform these defects to divacancy complex because of the very short distance between the vacancies in few nanometers SiC NPs [28]. Thus, divacancies can be formed without the use of any strongly invasive irradiation techniques. On the other hand, the surface itself with 1-2 nm distance can also represent a strain field towards the divacancies that can influence its PL spectrum. Again, ensemble measurements on the PL spectrum of divacancies in this sample may reveal about the quality of divacancy quantum bits.

To represent the two scenarios we used two batches of samples. First, we created porous 3C SiC and irradiated by neutrons. The porous 3C SiC is then used to create NPs by
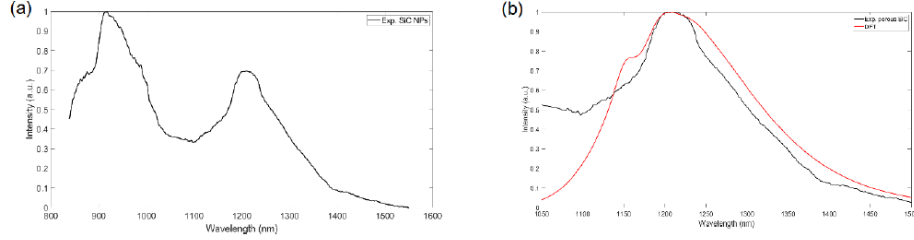
12

Figure 5. Room-temperature PL emission spectra as obtained by DFT calculations (red curve) and experiments fo the porous SiC sample (blue curve). Both spectra are normalized for the sake of comparison.

ultrasonication and filtering but we skipped this step in order to keep it in dry for processing with neutron irradiation. The advantage of neutron species compared to other ones like ions is that the whole porous sample is uniformly exposed to the irradiation to form vacancies. Second, we created divacancies in few nanometers 3C SiC NPs by means of chemistry as explained above. Finally, room temperature PL spectrum was recorded for both samples in our experiments because they should operate at room temperature as ODMR biomarkers.

The PL spectrum of porous 3C SiC is plotted in Fig. 5(a). We found background emission of other defects with a local maximum intensity at about 950 nm which has some overlap with the PL signal of divacancies around the position of the ZPL peak (invisible in experiment at room temperature). In our paper, we focus on the analysis of the divacancies' PL spectrum which may have low overlap at the highest intensity in PSB. By comparing this spectrum with the reference PL spectrum in Fig. 3, a shift is visible in the emission spectrum. In order to quantify it, we took the simulation spectrum at room temperature (Fig. 4) and then shifted the entire spectrum in the energy region to closely reproduce the experimental spectrum taken from the porous SiC [see Fig. 5(b)]. We obtain $+44$ nm (-38.41 meV) redshift.

The PL spectrum of 3C SiC NPs is plotted in Fig. 6. Here, we have no overlap from other defects as expected from the nature of creation of the defect. We applied the same fitting procedure on the simulated PL spectrum as explained above for that of porous SiC. We obtain -8 nm ($+7.30$ meV) blueshift in this process.

We find that shift parameter in the simulated PL spectrum of the NP samples is favorable over that of the neutron irradiated porous samples and no residual fluorescence is observable.
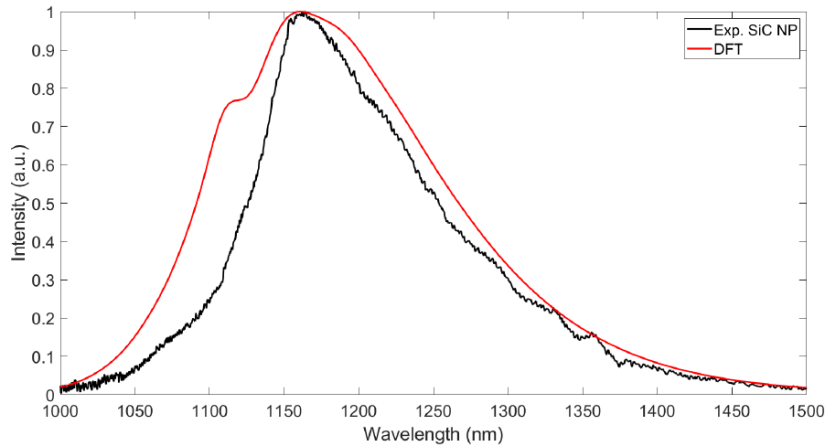
Figure 6. Room-temperature PL emission spectra as obtained by DFT calculations (red curve) and experiments for SiC NPs (blue curve). Both spectra are normalized for the sake of comparison.

This implies that our chemistry process produces higher quality divacancy quantum bits in ultrasmall 3C SiC NPs than those from traditional irradiation techniques.

IV.   SUMMARY

We analyzed the PL spectrum of divacancies in 3C SiC. We find that the Debye-Waller factor is indeed favorable (about 7%) over that of other divacancy configurations in 4H SiC as previous experimental date implied [16]. We identified the origin of the highest intensity in the phonon sideband which is an overlap of motion of the nearest neighbor carbon and silicon atoms around the vacancies. Our analysis indicates that ZPL linewidth faster broadens at elevated temperatures than that of NV center in diamond. By having a relatively good accuracy in the simulated PL spectrum we applied this to interpret the PL spectrum of divacancies recorded in neutral irradiated porous 3C SiC and in few nanometers diameter 3C SiC NPs. We find that the chemistry method produces higher quality of divacancy quantum bits than irradiation technique does. These results are very encouraging towards single defect detection of divacancies and characterization of their spin properties in few nanometers 3C SiC NPs.

V. ACKNOWLEDGEMENTS

[1] G. Zhang, Y. Cheng, J.-P. Chou, and A. Gali, Applied Physics Reviews **7**, 031308 (2020), publisher: American Institute of Physics.

[2] G. Wolfowicz, F. J. Heremans, C. P. Anderson, S. Kanai, H. Seo, A. Gali, G. Galli, and D. D. Awschalom, Nature Reviews Materials **6**, 906 (2021), publisher: Nature Publishing Group.

[3] S. Castelletto, B. C. Johnson, V. Ivády, N. Stavrias, U. T., A. Gali, and T. Oshima, Nat. Mater. **13**, 151 (2013).

[4] A. Lohrmann, N. Iwamoto, Z. Bodrog, S. Castelletto, T. Ohshima, T. J. Karle, A. Gali, P. S., J. C. McCallum, and B. C. Johnson, Nat. Comm. **6**, 7783 (2015).

[5] M. Widmann, S.-Y. Lee, T. Rendler, N. T. Son, H. Fedder, S. Paik, L.-P. Yang, N. Zhao, S. Yang, I. Booker, A. Denisenko, M. Jamali, S. A. Momenzadeh, I. Gerhardt, T. Ohshima, A. Gali, E. Janzén, and J. Wrachtrup, Nature Materials **14**, 164 (2015).

[6] D. J. Christle, A. L. Falk, A. P., P. V. Klimov, J. Ul Hassan, N. T. Son, J. E., O. T., and D. D. Awschalom, Nat. Mater. **14**, 164 (2015).

[7] M. Radulaski, M. Widmann, M. Niethammer, J. L. Zhang, S.-Y. Lee, T. Rendler, K. G. Lagoudakis, N. T. Son, E. Janzén, T. Ohshima, J. Wrachtrup, and J. Vučković, Nano Letters **17**, 1782 (2017), pMID: 28225630, https://doi.org/10.1021/acs.nanolett.6b05102.

[8] S.-Y. Lee, M. Niethammer, and J. Wrachtrup, Phys. Rev. B **92**, 115201 (2015).

[9] H. Kraus, V. A. Soltamov, F. Fuchs, D. Simin, A. Sperlich, P. G. Baranov, G. V. Astakhov, and V. Dyakonov, Scientific Reports **4**, 10.1038/srep05303 (2014).

[10] D. Simin, V. A. Soltamov, A. V. Poshakinskiy, A. N. Anisimov, R. A. Babunts, D. O. Tolmachev, E. N. Mokhov, M. Trupke, S. A. Tarasenko, A. Sperlich, P. G. Baranov, V. Dyakonov,

and G. V. Astakhov, Physical Review X **6**, 031014 (2016).

[11] D. Simin, F. Fuchs, H. Kraus, A. Sperlich, P. G. Baranov, G. V. Astakhov, and V. Dyakonov, Physical Review Applied **4**, 014009 (2015).

[12] M. Niethammer, M. Widmann, S.-Y. Lee, P. Stenberg, O. Kordina, T. Ohshima, N. T. Son, E. Janzén, and J. Wrachtrup, Physical Review Applied **6**, 034001 (2016).

[13] C. J. Cochrane, J. Blacksberg, M. A. Anders, and P. M. Lenahan, Scientific Reports **6**, 37077 (2016).

[14] A. N. Anisimov, D. Simin, V. A. Soltamov, S. P. Lebedev, P. G. Baranov, G. V. Astakhov, and V. Dyakonov, Scientific Reports **6**, 33301 (2016).

[15] W. F. Koehl, B. B. Buckley, F. J. Heremans, G. Calusine, and D. D. Awschalom, Nature **479**, 84 (2011).

[16] D. J. Christle, P. V. Klimov, C. F. de las Casas, K. Szász, V. Ivády, V. Jokubavicius, J. Ul Hassan, M. Syväjärvi, W. F. Koehl, T. Ohshima, N. T. Son, E. Janzén, A. Gali, and D. D. Awschalom, Phys. Rev. X **7**, 021046 (2017).

[17] P. G. Baranov, I. V. Il'in, E. N. Mokhov, M. V. Muzafarova, S. B. Orlinskii, and J. Schmidt, Jounal of Experimental and Theoretical Physics Letters **82**, 441 (2005).

[18] N. T. Son, P. Carlsson, J. ul Hassan, E. Janzén, T. Umeda, J. Isoya, A. Gali, M. Bockstedte, N. Morishita, T. Ohshima, and H. Itoh, Phys. Rev. Lett. **96**, 055501 (2006).

[19] V. Y. Bratus, R. S. Melnik, S. M. Okulov, V. N. Rodionov, B. D. Shanina, and M. I. Smoliy, Physica B: Condensed Matter **404**, 4739 (2009).

[20] A. Gali, A. Gällström, N. T. Son, and E. Janzén, Materials Science Forum **645-648**, 395 (2010).

[21] A. Gali, physica status solidi (b) **248**, 1337 (2011).

[22] N. T. Son, E. Sörman, W. M. Chen, C. Hallin, O. Kordina, B. Monemar, E. Janzén, and J. L. Lindström, Physical Review B **55**, 2863 (1997), publisher: American Physical Society.

[23] E. Janzén, A. Henry, J. P. Bergman, A. Ellison, and B. Magnusson, Materials Science in Semiconductor Processing Advanced Characterisation of Semiconductor Materials, **4**, 181 (2001).

[24] W. E. Carlos, N. Y. Garces, E. R. Glaser, and M. A. Fanton, Physical Review B **74**, 235201 (2006).

[25] A. M. Smith, M. C. Mancini, and S. Nie, Nature Nanotechnology **4**, 710 (2009).

[26] B. Somogyi, V. Zólyomi, and A. Gali, Nanoscale **4**, 7720 (2012).

[27] B. Somogyi and A. Gali, Journal of Physics: Condensed Matter **26**, 143202 (2014).

[28] D. Beke, J. Valenta, G. Károlyházy, S. Lenk, Z. Czigány, B. G. Márkus, K. Kamarás, F. Simon, and A. Gali, The Journal of Physical Chemistry Letters **11**, 1675 (2020), publisher: American Chemical Society.

[29] K. Huang, A. Rhys, and N. F. Mott, Proceedings of the Royal Society of London. Series A. Mathematical and Physical Sciences **204**, 406 (1950), https://royalsocietypublishing.org/doi/pdf/10.1098/rspa.1950.0184.

[30] A. Alkauskas, B. B. Buckley, D. D. Awschalom, and C. G. V. de Walle, New Journal of Physics **16**, 073026 (2014).

[31] A. Gali, D. T., M. Vörös, G. Thiering, E. Cannuccia, and A. Marini, Nat. Comm. **7**, 11327 (2016).

[32] D. Beke, G. Károlyházy, Z. Czigány, G. Bortel, K. Kamarás, and A. Gali, Scientific Reports **7**, 1 (2017).

[33] A. Csóré, I. G. Ivanov, N. T. Son, and A. Gali, Photoluminescence lineshapes and charge state control of divacancy qubits in silicon carbide (2021), arXiv:2107.01971 [cond-mat.mes-hall].

[34] P. Debye, Annalen der Physik **348**, 49 (1913).

[35] I. Waller, Zeitschrift fur Physik **17**, 398 (1923).

[36] K.-M. C. Fu, C. Santori, P. E. Barclay, L. J. Rogers, N. B. Manson, and R. G. Beausoleil, Physical Review Letters **103**, 256404 (2009).

[37] J. Heyd, G. E. Scuseria, and M. Ernzerhof, The Journal of Chemical Physics **118**, 8207 (2003).

[38] A. Gali, E. Janzén, P. Deák, G. Kresse, and E. Kaxiras, Phys. Rev. Lett. **103**, 186404 (2009).

[39] P. E. Blöchl, Phys. Rev. B **50**, 17953 (1994).

[40] G. Kresse and J. Furthmüller, Phys. Rev. B **54**, 11169 (1996).

[41] I. B. Bersuker, The Jahn-Teller effect (Cambridge University Press, 2006).

[42] J. P. Perdew, K. Burke, and M. Ernzerhof, Phys. Rev. Lett. **77**, 3865 (1996).

[43] R. J. Bell, P. Dean, and D. C. Hibbins-Butler, Journal of Physics C: Solid State Physics **3**, 2111 (1970).

[44] G. Thiering and A. Gali, Physical Review B **96**, 081115 (2017).

[45] B. Magnusson, N. T. Son, A. Csóré, A. Gällström, T. Ohshima, A. Gali, and I. G. Ivanov, Phys. Rev. B **98**, 195202 (2018).

[46] A. L. Falk, B. B. Buckley, G. Calusine, W. F. Koehl, V. V. Dobrovitski, A. Politi, C. A. Zorman, P. X.-L. Feng, and D. D. Awschalom, Nat Commun **4**, 1819 (2013).

[47] J.-F. Wang, F.-F. Yan, Q. Li, Z.-H. Liu, J.-M. Cui, Z.-D. Liu, A. Gali, J.-S. Xu, C.-F. Li, and G.-C. Guo, Nature Communications **12**, 3223 (2021).